REPORT DOCUMENTATION PAGE

2

Form Approved OMB NO. 0704-0188

1. REPORT DATE (DD-MM-YYYY)	2. REPORT TYPE	3. DATES COVERED (From - To)
	New Reprint	-

4. TITLE AND SUBTITLE

Highly Adsorptive, MOF-Functionalized Nonwoven Fiber Mats for Hazardous Gas Capture Enabled by Atomic Layer Deposition

5a. CONTRACT NUMBER

W911NF-13-1-0173

5b. GRANT NUMBER

5c. PROGRAM ELEMENT NUMBER

6. AUTHORS

Junjie Zhao, Mark D. Losego, Paul C. Lemaire, Philip S. Williams, Bo Gong, Sarah E. Atanasov, Trent M. Blevins, Christopher J. Oldham, Howard J. Walls, Sarah D. Shepherd, Matthew A. Browe, Gregory W. Peterson, Gregory N. Parsons

5d. PROJECT NUMBER

5e. TASK NUMBER

5f. WORK UNIT NUMBER

7. PERFORMING ORGANIZATION NAMES AND ADDRESSES

North Carolina State University
2701 Sullivan Drive
Suite 240, Campus Bx 7514
Raleigh, NC 27695 -7003

8. PERFORMING ORGANIZATION REPORT NUMBER

9. SPONSORING/MONITORING AGENCY NAME(S) AND ADDRESS (ES)

U.S. Army Research Office
P.O. Box 12211
Research Triangle Park, NC 27709-2211

10. SPONSOR/MONITOR'S ACRONYM(S)

ARO

11. SPONSOR/MONITOR'S REPORT NUMBER(S)

63857-CH.2

12. DISTRIBUTION AVAILIBILITY STATEMENT

Approved for public release; distribution is unlimited.

13. SUPPLEMENTARY NOTES

The views, opinions and/or findings contained in this report are those of the author(s) and should not contrued as an official Department of the Army position, policy or decision, unless so designated by other documentation.

14. ABSTRACT

While metal-organic frameworks (MOFs) show great potential for gas adsorption and storage, their powder form limits deployment opportunities. Integration of MOFs on polymeric fibrous scaffolds will enable new applications in gas adsorption, membrane separation, catalysis, and toxic gas sensing. Here, we demonstrate a new synthesis route for growing MOFs on fibrous materials that achieves high MOF loadings, large surface areas and high adsorptive capacities. We find that a nanoscale coating of Al2O3 formed by atomic layer deposition (ALD) on the surface of nonwoven fiber mats facilitates nucleation of MOFs on the fibers throughout the mat. Functionality of

15. SUBJECT TERMS

metal-organic frameworks; fibers; atomic layer deposition; adsorption; polymer

16. SECURITY CLASSIFICATION OF:			17. LIMITATION OF ABSTRACT	15. NUMBER OF PAGES	19a. NAME OF RESPONSIBLE PERSON
a. REPORT	b. ABSTRACT	c. THIS PAGE			Gregory Parsons
UU	UU	UU	UU		19b. TELEPHONE NUMBER 919-515-7553

Report Title

Highly Adsorptive, MOF-Functionalized Nonwoven Fiber Mats for Hazardous Gas Capture Enabled by Atomic Layer Deposition

ABSTRACT

While metal-organic frameworks (MOFs) show great potential for gas adsorption and storage, their powder form limits deployment opportunities. Integration of MOFs on polymeric fibrous scaffolds will enable new applications in gas adsorption, membrane separation, catalysis, and toxic gas sensing. Here, we demonstrate a new synthesis route for growing MOFs on fibrous materials that achieves high MOF loadings, large surface areas and high adsorptive capacities. We find that a nanoscale coating of Al2O3 formed by atomic layer deposition (ALD) on the surface of nonwoven fiber mats facilitates nucleation of MOFs on the fibers throughout the mat. Functionality of MOFs is fully maintained after integration, and MOF crystals are well attached to the fibers. Breakthrough tests for HKUST-1 MOFs [Cu3(BTC)2] on ALD-coated polypropylene fibers reveal NH3 dynamic loadings up to 5.93 ± 0.20 mol/kg (MOF+fiber). Most importantly, this synthetic approach is generally applicable to a wide range of polymer fibers (e. g., PP, PET, cotton) and MOFs (e.g., HKUST-1, MOF-74, and UiO-66).

REPORT DOCUMENTATION PAGE (SF298)
(Continuation Sheet)

Continuation for Block 13

ARO Report Number 63857.2-CH
Highly Adsorptive, MOF-Functionalized Nonwov...

Block 13: Supplementary Note

Approved for public release; distribution is unlimited.

Highly Adsorptive, MOF-Functionalized Nonwoven Fiber Mats for Hazardous Gas Capture Enabled by Atomic Layer Deposition

*Junjie Zhao, Mark D. Losego, Paul C. Lemaire, Philip S. Williams, Bo Gong, Sarah E. Atanasov, Trent M. Blevins, Christopher J. Oldham, Howard J. Walls, Sarah D. Shepherd, Matthew A. Browe, Gregory W. Peterson, and Gregory N. Parsons**

While metal-organic frameworks (MOFs) show great potential for gas adsorption and storage, their powder form limits deployment opportunities. Integration of MOFs on polymeric fibrous scaffolds will enable new applications in gas adsorption, membrane separation, catalysis, and toxic gas sensing. Here, we demonstrate a new synthesis route for growing MOFs on fibrous materials that achieves high MOF loadings, large surface areas and high adsorptive capacities. We find that a nanoscale coating of Al_2O_3 formed by atomic layer deposition (ALD) on the surface of nonwoven fiber mats facilitates nucleation of MOFs on the fibers throughout the mat. Functionality of MOFs is fully maintained after integration, and MOF crystals are well attached to the fibers. Breakthrough tests for HKUST-1 MOFs [$Cu_3(BTC)_2$] on ALD-coated polypropylene fibers reveal NH_3 dynamic loadings up to 5.93 ± 0.20 mol/kg$_{(MOF+fiber)}$. Most importantly, this synthetic approach is generally applicable to a wide range of polymer fibers (e.g., PP, PET, cotton) and MOFs (e.g., HKUST-1, MOF-74, and UiO-66).

1. Introduction

Hazardous gas adsorption has important implications for human health, industrial safety, and environmental protection. Traditional adsorbents including zeolites, activated carbons, and silica gels can abate hazardous gas emission, but there is growing need for materials with higher capacity and better selectivity, while simultaneously providing multifunctional performance (i.e. capture and alert capability).[1,2] Metal organic frameworks (MOFs), composed of metal-containing units and organic bridging ligands,[3] exhibit high surface area, good thermal stability, and have significant synthetic versatility, enabling structures with tunable pore sizes and adjustable internal functionality.[4] MOF synthesis usually follows wet solvothermal batch methods, producing powders that require further manipulation and handling, and may be difficult to implement for some applications.[5] Integration of MOFs on polymeric fibrous scaffolds could simplify handling, regeneration and deployment. It could also broaden practical use for filtration, separations, catalysis, sensing and other applications.[6]

Several methods have been used to integrate MOF crystals on polymer fiber matrices, including encapsulation in electrospun fibers [7,8] and immobilization on fibers via solvothermal synthesis,[9,10] layer-by-layer method [6,11] or microwave irradiation.[12] Unfortunately, these methods generally lead to small MOF loading fractions, poor MOF crystal quality, and low Brunauer–Emmett–Teller (BET) surface areas—limiting applicability. For example, Kuesgens *et al.* grew HKUST-1 crystals on pulp fibers using direct solvothermal synthesis and found the surface area to be limited to 314 m^2/g.[9] Wu *et al.* encapsulated HKUST-1 MOFs in electrospun fibers, and also only achieved a value of 311 m^2/g before repeating secondary growth.[8] These values are at least 2 times lower than pure HKUST-1 powders grown solvothermally (692–1460 m^2/g).[13–17] To date, no prior report has assessed the hazardous gas adsorption capacity for MOF-functionalized fibers.

In this work, we introduce a novel synthesis route for achieving high-quality MOF growth on polymer fibers. We use atomic layer deposition (ALD) to form a nanoscale-thick conformal coating on polymer fibers for nucleation of solvothermally grown MOF crystals. This approach is first demonstrated

J. Zhao, Dr. M. D. Losego, P. C. Lemaire, Dr. P. S. Williams, Dr. B. Gong, S. E. Atanasov, T. M. Blevins, Dr. C. J. Oldham, Prof. G. N. Parsons
Department of Chemical and Biomolecular Engineering
North Carolina State University, 911 Partners Way,
Raleigh, NC, 27695, USA
E-mail: gnp@ncsu.edu
Dr. H. J. Walls, S. D. Shepherd
RTI International, 3040 East Cornwallis Road
Research Triangle Park,
NC, 27709, USA
M. A. Browe, G. W. Peterson
Edgewood Chemical Biological Center
5183 Blackhawk Road, Aberdeen Proving Ground,
MD, 21010, USA

DOI: 10.1002/admi.201400040

with HKUST-1 on ALD-Al_2O_3-coated polypropylene fibers. MOF nucleation on fibers is compared between untreated and ALD-coated substrates, while the quality of MOFs is benchmarked to pure powders. Hazardous gas (ammonia) adsorption capacity was characterized via breakthrough tests. We also show the general applicability of this technique to a wide range of polymer fibers (e.g., PP, PET, and cotton) and MOFs (e.g., HKUST-1, MOF-74, and UiO-66).

2. Results and Discussion

Figure 1a–c illustrates the process scheme for the case of HKUST-1 grown on ALD-Al_2O_3-coated polypropylene fibers. Polypropylene (PP) fibers (Figure 1a) in a nonwoven mat were conformally coated with ALD Al_2O_3 (200 cycles at 60 °C), creating a core/shell "PP/ALD" structure with hydroxyl surface termination (Figure 1b).[18] This ALD coating can change wettability of fibers for thorough permeation of solvothermal solvents (Figure S1),[17] and improve reactivity of the fiber surfaces for MOF nucleation.[19] Depending on the the deposition conditions, ALD coatings can increase surface roughness,[20] which may also promote MOF nucleation. HKUST-1 [$Cu_3(BTC)_2$] was grown onto ALD-coated fibers solvothermally using copper nitrate trihydrate and 1,3,5-benzenetricarboxylic (BTC) acid as precursors in a water/ethanol (50/50 vol%) solution (Figure 1c). Fiber mats were placed in a Teflon-lined pressure vessel and immersed in the liquid reagents which readily wetted the coated fiber substrates. The vessel was sealed, and MOF growth proceeded under the optimal condition at 120 °C for 20 hours (optimization shown in the Supporting Information). Figure 1d shows HKUST-1 cyrstals grown densely and conformally on an ALD-coated PP fibers. This resulting MOF-functionalized fiber mat is referred to as "MOF-PP/ALD".

In **Figure 2** we compare the growth of HKUST-1 on untreated and ALD-coated PP fiber mats. MOFs grown on the untreated PP fibers (referred to as "MOF-PP") show macroscopic non-uniformity and appear to have nucleated homogeneously (i.e. in solution) throughout the fiber matrix (Figure 2a). When coated with ALD Al_2O_3, the fiber mats show uniform MOF coverage indicative of heterogeneous nucleation on the fiber surface (Figure 2b). X-ray diffraction data in Figure 2c confirms HKUST-1 crystal formation for both structures.

Figure 2d shows the percent mass increase after MOF growth on untreated and ALD-coated PP fiber substrates. Mass increase percentage ($\Delta m/m_0$) is 336 ± 38% for PP/ALD, and 228 ± 83% for untreated PP respectively. The results show that the ALD treatment enhances both the amount and uniformity of MOF growth. Normalizing the MOF mass loading per unit substrate external surface area, we find Δm = 14.78 mg/cm^2 on PP/ALD to be 54% larger than on untreated PP (Δm = 9.61 mg/cm^2). Mass gain is also more reproducible on the ALD-Al_2O_3-coated fiber mats, as indicated by the box-plot's interquartile range (IQR) = 69% for PP/ALD vs 145% for untreated PP. Figure 2e shows results from N_2 isotherms and Brunauer–Emmett–Teller (BET) surface area analysis. The MOF-PP/ALD fiber mats show an average surface area ($SA_{MOF+fiber}$) of 695 ± 76 m^2/$g_{(MOF+fiber)}$, which is ~60% higher than that of MOF-PP fibers (434 ± 198 m^2/$g_{(MOF+fiber)}$). This is consistent with the higher MOF mass gain on PP/ALD substrates. The surface area of MOF-PP/ALD fiber mat is also >2× larger than prior reports for MOFs on fibers.[8,9]

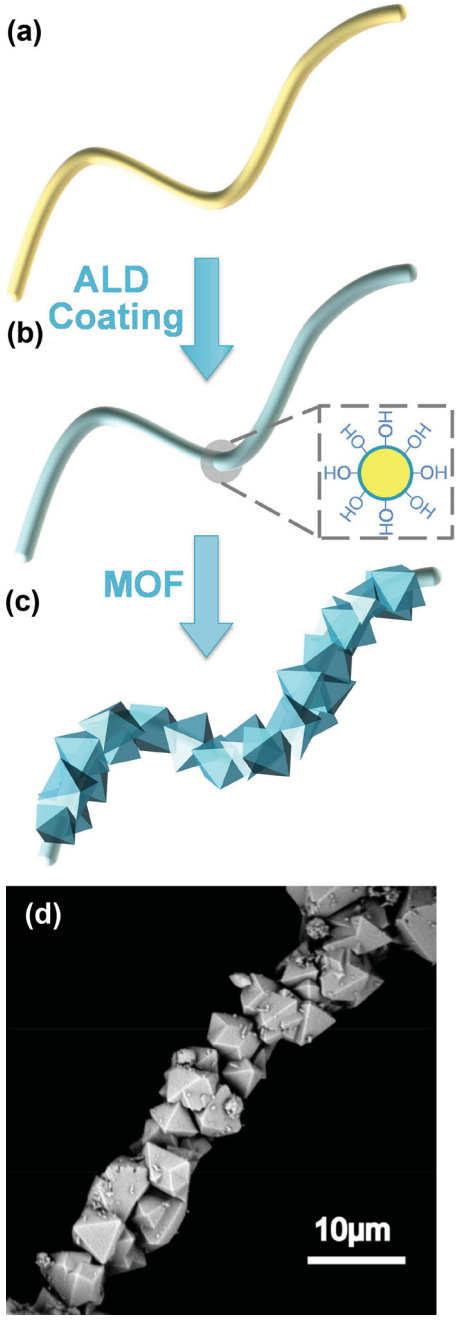

Figure 1. a-c) Schematic illustration of the synthesis route. a) Polymer fiber substrate. b) Al_2O_3-coated polymer fiber via atomic layer deposition (ALD). The cross section in the dashed square illustrates the conformal coating of ALD Al_2O_3 with hydroxyl surface termination. c) MOFs integated on Al_2O_3-coated polymer fiber using solvothermal MOF synthesis. d) SEM image of HKUST-1 MOF crystals grown on an ALD-Al_2O_3-coated polypropylene fiber (MOF-PP/ALD).

We compare the quality of the MOFs nucleated on fibers to that of pure powders. The surface area of the MOF component in the MOF-fiber material (SA_{MOF}) is given by:

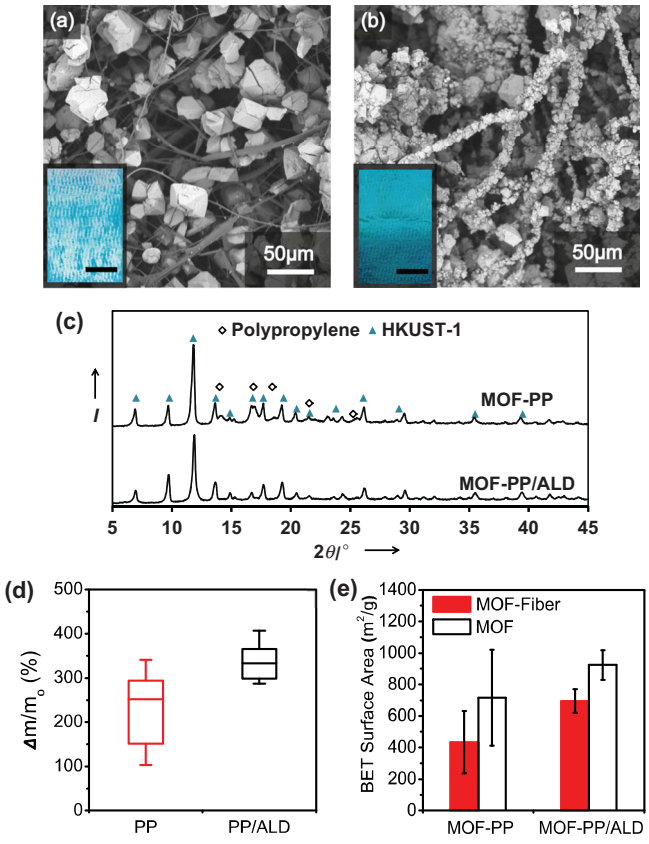

Figure 2. Comparison of HKUST-1 MOF grown on untreated and ALD-coated polypropylene fiber mats. a) SEM image of HKUST-1 MOF grown on untreated polypropylene fiber mats (MOF-PP). Insert image is a photograph of MOF-PP (scale bar represents 1cm). b) SEM image of HKUST-1 MOF grown on ALD-Al_2O_3-coated polypropylene fiber mats (MOF-PP/ALD). Insert image is a photograph of MOF-PP/ALD (scale bar represents 1 cm). c) X-ray diffraction of MOF-PP and MOF-PP/ALD. d) Mass increase percentage based on substrate dry weight. Interquartile range and average value were calculated based on 16 MOF-PP samples and 12 MOF-PP/ALD samples. e) Brunauer–Emmett–Teller (BET) surface area of MOF-fiber materials and calculated BET surface area for MOF part (error bars represent standard deviation). BET surface area for PP fiber substrates is 1.3~1.5 m^2/g. The values were measured for uncoated and ALD coated fibers, and the values were indistinguishable.

$$SA_{MOF} \approx \frac{SA_{MOF+fiber} \times m_{MOF+fiber} - SA_{fiber} \times m_{fiber}}{m_{MOF+fiber} - m_{fiber}} \quad (1)$$

where SA is the surface area and m is the mass of each component. From this analysis (Figure 2e), we find SA_{MOF} = ~716 ± 305 $m^2/g_{(MOF)}$ for MOF-PP, while SA_{MOF} = 924 ± 94 $m^2/g_{(MOF)}$ for MOF-PP/ALD. HKUST-1 powders similarly produced in our lab show SA_{MOF} = 1066 m^2/g. It is consistent with as-synthesized high quality HKUST-1 crystals,[13–17] and essentially similar to the MOFs we grew on PP/ALD fibers. Although post-synthesis activation maybe further increases the MOF surface area, vacuum drying at high temperature is not suitable for the polymer fiber substrate. Lower surface area on untreated PP is likely the result of nonstoichiometric crystal phases or other unwanted side products.

To assess the quality of interaction between MOFs and the fiber substrates, we performed compressed air blowing tests. We forced compressed air at ~40 psi for 4 min through a standard-size MOF-fiber mat (10 cm^2) and measured the mass change versus air-flow time. Results are plotted in Figure S5. Generally, the mass loss stabilizes within a few minutes, and the overall loss of MOF-PP/ALD is limited to ~15% of the starting mass. Many samples show >85% MOF retention. Subsequent laboratory handling of MOF-fiber mats after forced air testing resulted in no noticeable MOF detachment. In addition, we tested our MOF-fiber mats in bending and rubbing tests. The amount of particles coming off during these tests was too small to quatify. Rubbing test may also lead to fiber abrasion. So compressed air blowing test was chosen to be our standard methods for MOF attachement testing.

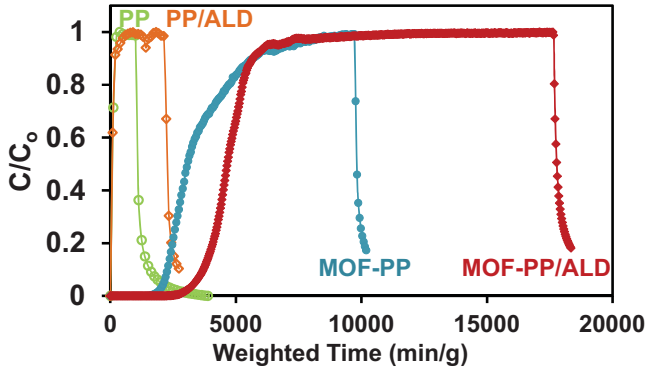

Figure 3. NH_3 breakthrough curves for untreated polypropylene fiber mats (PP, ○), ALD-Al_2O_3-coated polypropylene fiber mats (PP/ALD, ◇), HKUST-1 MOF grown on untreated polypropylene fiber mats (MOF-PP, ●), HKUST-1 MOF grown on ALD-Al_2O_3-coated polypropylene fiber mats (MOF-PP/ALD, ◆).

To evaluate MOF-functionalized fibers for hazardous gas adsorption, we used ammonia breakthrough analysis (Figure S6).[21] Results in **Figure 3** show downstream NH_3 concentration changes as a function of time after the feed flow starts. Ammonia breakthrough is defined as the time at which the downstream signal reaches 5% of the feed concentration. Dynamic loading (calculation shown in the Supporting Information) indicates the total ammonia sorption capacity at saturation. The decay in NH_3 signal after feed flow is terminated shows NH_3 desorption rate, indicating the retention and therefore strength of sorption. Figure 3 shows that the breakthrough time for MOF-PP/ALD is up to 58% longer than MOF-PP. Control PP mats without MOFs exhibit immediate breakthrough. From the breakthrough results, the ammonia dynamic loadings are 5.28 ± 0.40 $mol_{NH3}/kg_{(MOF+fiber)}$ for MOF-PP/ALD and 4.57 ± 0.27 $mol_{NH3}/kg_{(MOF+fiber)}$ for MOFs on untreated fibers. Calculation results show the NH_3 dynamic loading for the MOF component in MOF-PP/ALD fiber mats is 6.9 ± 0.5 mol/$kg_{(MOF)}$, similar to that for pure MOF powders synthesized in our lab (7.23 mol/kg) and consistent with the reported values.[16] The similar values for the NH_3 dynamic loadings indicate the adsorption takes place in the bulk MOF crystals on the fibers.

In addition to ammonia, we also evaluated the performance of MOF-functionalized fibers for H_2S removal. Compared with H_2S adsorption by MOF powders,[22] the H_2S dynamic loading for our MOF-fiber mats show good H_2S loading capacity, demonstrating that the MOF-fiber constructs have functional capacity to adsorb hazardous gases beyond NH_3.

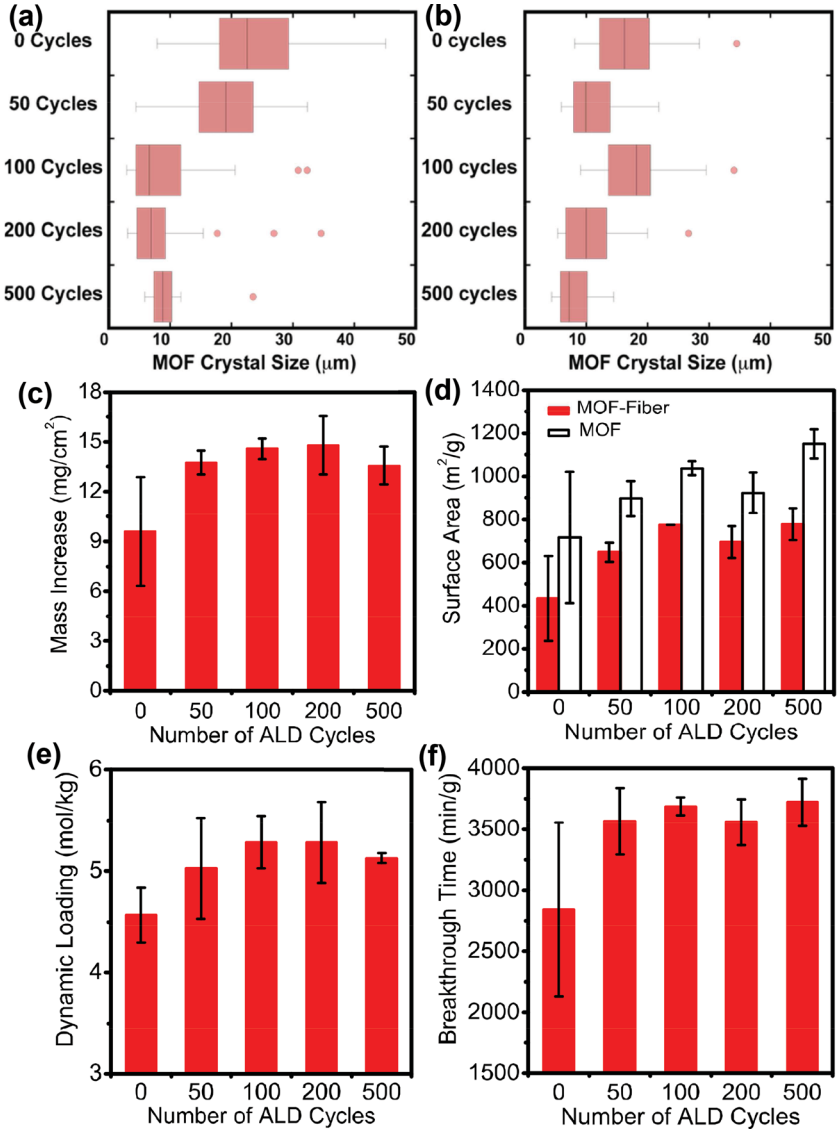

Figure 4. MOF-fiber mats with different ALD coating thicknesses. a) MOF crystal size distribution on the top surface. b) MOF crystal size distribution on the cross-section. Crystal size distributions were analyzed based on 50 measured crystal sizes on each corresponding SEM image. c) Mass increase of the fiber mats after MOF integration. d) BET surface area of the MOF-functionalized fiber mats and the surface area of MOF component in the fiber mats. e) NH_3 dynamic loading on MOF-functionalized fiber mats. f) NH_3 breakthrough time on MOF-functionalized fiber mats.

We investigated the effect of ALD coating thickness, and find that MOF crystal size distribution and extent of growth into the fiber mat can be systematically changed with ALD thickness. Figure S7 shows top-view and cross-sectional SEM images of MOFs grown on PP fiber mats with 0, 50, 100, 200 and 500 cycles of Al_2O_3 ALD (roughly correspond to 0 nm, 6 nm, 12 nm, 24 nm, and 60 nm of Al_2O_3 respectively). MOF crystal size distributions analyzed from both top-view and cross-sectional SEM are plotted in **Figure 4**a,b and Figure S8. On the top layer of fibers (Figure 4a), MOF crystal sizes decrease from 24 ± 8 μm to 9 ± 3μm with narrowing distributions, as ALD coating thickness increases from 0 to 500 cycles. Similar trend is also found in the cross-sections of the MOF-fiber mats with different ALD thickness (Figure 4b). The amount of MOFs grown into the fiber mat rises as the number of ALD cycles increases to ~100 cycles (Figure S7), leading to the similar trends of MOF loading and BET surface area shown in Figure 4c,d. The NH_3 breakthrough tests, summarized in Figure 4e,f show that NH_3 adsorption capacity correlates closely with BET surface area, regardless of the different crystal size distribution.

In addition to ALD coating thickness, we also tested the effect of ALD chemistry. ALD ZnO and TiO_2 coated PP fiber mats were functionalized with HKUST-1 MOFs, and the results shown in **Figure 5**a,b are compared with MOFs on ALD Al_2O_3 coated PP. We find that MOF crystals on ZnO are small, whereas those on TiO_2 are generally larger than the MOFs on Al_2O_3. This indicates that MOF crystal morphology can be adjusted using different ALD coatings. We hypothesize that the wettability, surface roughness and isoelectric points (IEP) of different ALD coatings may all affect the nucleation of MOF crystals. The mechanism of MOF nucleation on different ALD materials is currently under investigation. The resulting mass increase, BET surface area, and NH_3 dynamic loading of these MOF-fiber materials are shown in **Table 1**. The NH_3 dynamic loading of MOF-PP/ALD(ZnO) (5.93 ± 0.20 $mol/kg_{(MOF+fiber)}$) represents the best adsorptive capacity of MOF-fiber materials so far. MOF-PP/ALD(TiO_2) fiber mats exhibit less adsorptive capacity than MOF-PP/ALD(Al_2O_3) and MOF-PP/ALD(ZnO). This may be explained with the low surface area of the MOF component in this material (~670 $m^2/g_{(MOF)}$), which may suggest the formation of impurities or the necessity of careful post-synthesis activation.

Finally, we demonstrate our approach can readily extend to various fibers and MOFs. Figure 5d,e and Table 1 show HKUST-1 growth on ALD Al_2O_3 coated polybutylene terephthalate (PBT) and cotton fiber mats. Cotton cellulose has hydroxyl groups that promote ALD Al_2O_3 growth,[23] but our results show HKUST-1 mass uptake on ALD treated cotton is less than on other ALD-modified fibers. Initial MOF loading on cotton/ALD fiber mats is comparable with that on PP/ALD and PBT/ALD fiber mats (Table 1), but MOFs grown on cotton/ALD fibers tend to show poor adhesion. We hypothesize that the ALD layer enhances nucleation, but nucleii attachement is less robust, possibly resulting from the smooth surface after ALD treatment. This is supported by Figures 5(e) and S9 showing MOF growth in the crevaces on the cotton fibers. The details of MOF nucleation on different surfaces are currently under investigation. Preliminary examples of Zn-MOF-74, Mg-MOF-74 and UiO-66 on ALD-coated

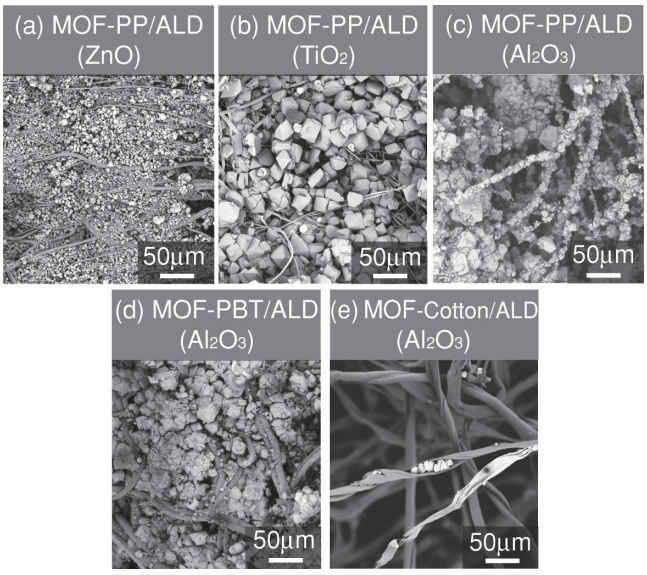

Figure 5. HKUST-1 MOF grown on different ALD coatings and different polymer fibers. a) SEM image of MOF on ALD-ZnO-coated polypropylene fiber mats (**MOF-PP/ALD(ZnO)**). b) SEM image of MOF on ALD-TiO_2-coated PP fiber mats (**MOF-PP/ALD(TiO_2)**). c) SEM image of MOF on ALD-Al_2O_3- coated PP fiber mats (**MOF-PP/ALD(Al_2O_3)**). d) SEM image of MOF on ALD-Al_2O_3-coated polybutylene terephthalate (PBT) fiber mats (**MOF-PBT/ALD(Al_2O_3)**). e) SEM image of MOF on ALD-Al_2O_3-coated cotton fiber mats (**MOF-Cotton/ALD(Al_2O_3)**).

nonwoven polymer fibrous substrates are given in Figure S10. Integration of these MOFs on nonwoven fiber mats could potentially broaden the practical use for filtration, separations, catalysis, sensing and other applications.

3. Conclusion

In conclusion, we have demonstrated a new synthesis route using ALD coatings to facilitate MOF nucleation on fibrous materials. Al_2O_3 ALD coatings improve the MOF macroscopic uniformity and its coverage on fiber surfaces. MOF-PP/ALD fiber mats exhibit higher BET surface areas and higher NH_3 dynamic loading capacities than MOFs grown on untreated PP fiber mats. These results significantly advance capability for functional MOFs on fiber substrates. Variations in ALD surface modification are found to affect MOF crystallite size and distribution but ultimately have minimal effect on ammonia removal performance. The process scheme presented here provides a robust platform technology for integrating various MOFs onto polymeric fibrous substrates for the use in human protection, industrial safety, and environmental preservation.

Table 1. Characterization of MOF-functionalized fiber mats: fiber mass gain (mg/cm^2) after MOF integration, BET surface area (m^2/g) of MOF-fiber materials and NH_3 dynamic loading (mol/kg) calculated from breakthrough curves.

MOF-fiber Composites	Fiber Mass Gain (mg/cm^2)	Total BET Surface Area (m^2/g)	NH_3 Dynamic Loading (mol/kg)
MOF-PP/ALD(ZnO)	25.21	764 ± 11	5.93 ± 0.20
MOF-PP/ALD(TiO_2)	12.85	509 ± 151	2.75 ± 0.02
MOF-PP/ALD(Al_2O_3)	14.78	694 ± 76	5.28 ± 0.40
MOF-PBT/ALD(Al_2O_3)	17.17	485	2.52 ± 0.23
MOF-Cotton/ALD(Al_2O_3)	13.59	121	1.70 ± 1.14

4. Experimental Section

Nonwoven polypropylene, polybutylene terephthalate and cotton fiber mats were used as received [23] (NCRC, NCSU) and coated with 200 cycles of ALD Al_2O_3 at 60 °C. HKUST-1 MOFs were synthesized using $Cu(NO_3)_2{\cdot}3H_2O$ (0.87 g, Aldrich, 99%) in ethanol (12 mL) and 1,3,5-benzene-tricarboxylic acid (0.42 g, Acros Organics, 98%) in deionized water (12 mL) as precursor solutions. Fiber mats were transfered in a Teflon-lined pressure vessel with the mixed precursor solution. MOF growth proceeded in the sealed vessel at 120 °C for 20 hours. After synthesis, the fiber mats were rinsed in ethanol, and dried in vacuum over at 120 °C for 12 hours. Scanning electron microscope (SEM) images were taken with an FEI Phenom bench-top SEM. Samples were sputter-coated with 5~10 nm of Au-Pd before imaging. X-ray diffraction (XRD) was measured with a Rigaku SmartLab X-ray diffraction tool (CuKα X-ray source). BET surface areas were measured using a Quantachrome Autosorb-1C surface area and pore size analyzer. Samples were degassed at 120 °C for 12 h before measurement. BET surface areas were analyzed based on N_2 isotherm adsorption within the P/P_o range of 0.05–0.31. Rapid micro-breakthrough analysis equipment (shown in Figure S6) was used to measure NH_3 adsorption (details and calculations are shown in the Supporting Information).

Supporting Information

Supporting Information is available from the Wiley Online Library or from the author.

Acknowledgements

The authors acknowledge funding from ECBC through grant #W911SR-07-C-0075 and from the Joint Science and Technology Office through Army Research Office grant #W911NF-13–1–0173.

Received: January 18, 2014
Revised: February 22, 2014
Published online: March 20, 2014

[1] J.-R. Li, R. J. Kuppler, H.-C. Zhou, *Chem. Soc. Rev.* **2009**, *38*, 1477.
[2] Z.-Z. Lu, R. Zhang, Y.-Z. Li, Z.-J. Guo, H.-G. Zheng, *J. Am. Chem. Soc.* **2011**, *133*, 4172.
[3] S. L. James, *Chem. Soc. Rev.* **2003**, *32*, 276.
[4] S. T. Meek, J. A. Greathouse, M. D. Allendorf, *Adv. Mater.* **2011**, *23*, 249.
[5] D. Bradshaw, A. Garai, J. Huo, *Chem. Soc. Rev.* **2012**, *41*, 2344.
[6] M. Meilikhov, K. Yusenko, E. Schollmeyer, C. Mayer, H.-J. Buschmann, R. A. Fischer, *Dalton Trans.* **2011**, *40*, 4838.
[7] R. Ostermann, J. Cravillon, C. Weidmann, M. Wiebcke, B. M. Smarsly, *Chem. Commun.* **2011**, *47*, 442.
[8] Y. Wu, F. Li, H. Liu, W. Zhu, M. Teng, Y. Jiang, W. Li, D. Xu, D. He, P. Hannam, G. Li, *J. Mater. Chem.* **2012**, *22*, 16971.
[9] P. Kuesgens, S. Siegle, S. Kaskel, *Adv. Eng. Mater.* **2009**, *11*, 93.

[10] M. Silva Pinto, C. A. Sierra-Avila, J. P. Hinestroza, *Cellulose* **2012**, *19*, 1771.
[11] A. R. Abbasi, K. Akhbari, A. Morsali, *Ultrason. Sonochem.* **2012**, *19*, 846.
[12] A. Centrone, Y. Yang, S. Speakman, L. Bromberg, G. C. Rutledge, T. A. Hatton, *J. Am. Chem. Soc.* **2010**, *132*, 15687.
[13] S. S. Chui, *Science* **1999**, *283*, 1148.
[14] S. Basu, M. Maes, A. Cano-Odena, L. Alaerts, D. E. De Vos, I. F. J. Vankelecom, *J. Membr. Sci.* **2009**, *344*, 190.
[15] D. Britt, D. Tranchemontagne, O. M. Yaghi, *Proc. Natl. Acad. Sci. U. S. A.* **2008**, *105*, 11623.
[16] G. W. Peterson, G. W. Wagner, A. Balboa, J. Mahle, T. Sewell, C. J. Karwacki, *J. Phys. Chem. C* **2009**, *113*, 13906.
[17] B. Levasseur, C. Petit, T. J. Bandosz, *ACS Appl. Mater. Interfaces* **2010**, *2*, 3606.
[18] G. K. Hyde, G. Scarel, J. C. Spagnola, Q. Peng, K. Lee, B. Gong, K. G. Roberts, K. M. Roth, C. A. Hanson, C. K. Devine, S. M. Stewart, D. Hojo, J.-S. Na, J. S. Jur, G. N. Parsons, *Langmuir* **2010**, *26*, 2550.
[19] D. Zacher, A. Baunemann, S. Hermes, R. A. Fischer, *J. Mater. Chem.* **2007**, *17*, 2785.
[20] J. S. Jur, J. C. Spagnola, K. Lee, B. Gong, Q. Peng, G. N. Parsons, *Langmuir* **2010**, *26*, 8239.
[21] T. G. Glover, G. W. Peterson, B. J. Schindler, D. Britt, O. Yaghi, *Chem. Eng. Sci.* **2011**, *66*, 163.
[22] C. Petit, B. Mendoza, T. J. Bandosz, *ChemPhysChem* **2010**, *11*, 3678.
[23] G. K. Hyde, K. J. Park, S. M. Stewart, J. P. Hinestroza, G. N. Parsons, *Langmuir* **2007**, *23*, 9844.